Use of Hot Spot Analysis to Detect Underground Coal Fires from Landsat-8 TIRS Data: A Case Study in the Khanh Hoa Coal Field, North-East of Vietnam

Thanh Tien Nguyen[1*] and Tuyen Danh Vu[2]

[1]*Faculty of Surveying, Mapping and Geographic Information, Hanoi University of Natural Resources and Environment, Hanoi 100000, Vietnam*

[2]*Department of Training, Hanoi University of Natural Resources and Environment, Hanoi 100000, Vietnam*

ARTICLE INFO

Received: 17 Sep 2018
Received in revised:
25 Dec 2018
Accepted: 22 Jan 2019
Published online:
21 Feb 2019
DOI: 10.32526/ennrj.17.3.2019.17

Keywords:
Underground coal fire detection/ Hotspot analysis/ Landsat-8 TIRS data/ Khanh Hoa coal field (Vietnam)

*** Corresponding author:**
E-mail:
tdgis_ntthanh@163.com

ABSTRACT

Underground coal fire (UCF) detection from remotely sensed data plays an important role in controlling and preventing the effects of coal fires and their environmental impact. The limitation of commonly used methods does not take into account spatial autocorrelation among observations. For solving this limitation, a method for UCF detection was proposed using hot spot analysis (HSA). Based on the radiative transfer equation (RTE), land surface temperatures (LSTs) were firstly retrieved from the Landsat-8 TIRS data. The degree of spatial clustering among these LSTs was measured using HSA. UCF areas were then delineated based on 99 percent confidence level of hot spot areas. These fires were finally validated using known UCF sites and cross-validated with the results extracted from the ASTER TIR image. It was found from a case study in the Khanh Hoa coal field (North-East of Vietnam); (i) UCFs were strongly correlated with known coal fires and were highly consistent with those obtained from the ASTER TIR data; (ii) a total fire area of 197 hectares was detected, of which the fire areas of low, medium, high and extremely high levels were 37.3, 47.3, 53.2 and 59.3 hectares respectively; (iii) these fires were mainly detected in the central area and at coal ash dump sites of the southern coal field. The results show HSA can be used to effectively detect UCFs.

1. INTRODUCTION

Coal fires are serious problems which occur on the surface and in underground coal seams (Du et al., 2015a). These fires are caused by the spontaneous combustion of coal during coal oxidation (Qi et al., 2015), natural events (lightning, forest fires and peat fires) and human activities (mining and domestic fires) (Du et al., 2015a). They not only cause severe environmental problems (Finkelman and Stracher, 2011) such as releasing greenhouse-relevant (CO_2, CH_4) and toxic gasses (NO_X, N_2O, CO and SO_2) (Kuenzer and Dech, 2014) and constituting a major cause of disaster (Saini et al., 2016), but also lead to the loss of a valuable coal resource (Kuenzer and Dech, 2014). For these reasons, coal fire detection has received comparatively much attention from scientists in most coal-producing countries in the world (Du et al., 2015a; Pandey et al., 2017; Su et al., 2017) including in Vietnam (Tran et al., 2010; Trinh and Zablotskii, 2017; Tuyen et al., 2016; Vu, 2013).

Coal fire detection typically incorporates the identification of changes in the LST (Du et al., 2015a). Conventionally, these LSTs can be achieved from ground-based handheld thermal infrared imagery (Kuenzer and Dech, 2014) and by drilling holes for temperature measurements (Huijun et al., 2018). Using these methods, LST measurements are done very close to the fire, but they are nearly impossible to gather enough data over large areas (Gangopadhyay et al., 2006) or in inaccessible areas. To overcome this limitation, airborne thermal infrared data acquired during the daytime and nighttime have been used to identify high-temperature targets against low-temperature backgrounds (Bhattacharya et al., 1991; Greene et al., 1969). However, due to the high cost involved in data acquisition by these airborne scanners, available free orbital images such as Landsat-5 TM, -7 ETM+, -8 TIRS, ASTER and NOAA-9 AVHRR have been widely used to detect coal fires by many authors (Abbas et al., 2015; Du et al., 2015a; Du et al., 2015b; Jiang et al., 2011; Singh et al., 2017; Song

and Kuenzer, 2017). Among these images, Landsat-8 TIRS is a high resolution thermal infrared data which has been successfully used to extract surface and UCF information in many coal fields around the world such as China's Wuda (Song et al., 2015) and Rujigou (Huo et al., 2014a; Huo et al., 2014b) and India's Jharia (Pal et al., 2016; Roy et al., 2015a; Roy et al., 2015b; Singh et al., 2017). Therefore, the Landsat-8 TIRS data was used to detect UCFs in this study.

Many coal fire detection methods have been developed for the Landsat thermal infrared (TIR) data such as the methods based on density slicing (Yang et al., 2005; Zhang et al., 1998), sub-pixel analysis (Chatterjee, 2006; Dozier, 1981), moving window (Kuenzer et al., 2007; Voigt et al., 2004), multiple field fusion (Kuenzer et al., 2012; Künzer et al., 2008) and the fixed-threshold approach (Chatterjee et al., 2010) (see Du et al. (2015b), Huo et al. (2015) and Huo and Jiang (2014b) for a detailed discussion). Most recently, based on an assumption of the attenuation of temperature along the coal fire's boundaries which generates considerable numbers of spots with extremely high gradient values, Du et al. (2015b) proposed a self-adaptive gradient-based thresholding method (SAGBT) for coal fire detection using ASTER thermal infrared data. By analyzing algorithm performance using nighttime TIR images and images from different seasons, Du et al. (2015a) found that SAGBT-derived fires matched fire spots measured in the field with an average offset of 32.44 m and a matching rate of 70-85%. However, all of the above mentioned methods do not account for any spatial autocorrelation (or spatial dependence) among the observations. In many cases, spatial variation is not random, but tends to follow a pattern (such as spatial clustering) in which variability decreases as distance decreases between points in space as stated by Tobler's First Law of Geography (Tobler, 1979). Therefore, it is important to take into account spatial autocorrelation in coal fire detection when separating thermal anomaly from a set of LSTs. Degree of spatial autocorrelation can be measured using spatial association statistics such as Getis-Ord's G_i^* Geary's C, spatial scan, Tango's C, and Moran's I (Nguyen, 2018; Nguyen et al., 2016). To evaluate the existence of spatial clustering in spatial autocorrelation, the Getis-Ord's G_i^* statistic-based HSA technique has been widely used in many fields of study such as spatial analyses of urban heat islands (Lu et al., 2015; Tran et al., 2017), environmental pollution (Ding et al., 2015; Obida et al., 2018) and health sciences (Stopka et al., 2017; Zhang and Tripathi, 2018). HSA helps to understand if an event would create spatial clusters, and if that clustering would affect the surrounding areas (Odland, 1988); while Getis-Ord's G_i^* can not only indicate the presence of local clustering, but also the clustering of locations and intensity as well (Cheng et al., 2018). It is therefore the aim of this study to detect UCFs using HSA by considering spatial autocorrelation among a set of LSTs retrieved from the Landsat-8 TIRS data.

2. METHODOLOGY

2.1 Description of study area

The Khanh Hoa coal field is a large coal field located in the north-west of Thai Nguyen city (North-east of Vietnam) (Figure 1). It extends latitudinally from 21°36′03″N to 21°37′58″N and longitudinally from 105°45′38″E to 105°47′38″E, occupying 420 hectares of land with estimated reserves of 59.3 million tonnes of coal. UCFs started burning in underground coal seams at depths of between 30-40 m in 2008 (Tuyen et al., 2016; Vu, 2013) and have been burning for more than 10 years. These fires have caused severe environmental problems (Vu, 2013), constitute a major cause of diseases such as lung cancer, and lead to the relocation of thousands of households. This serious geo-hazard has received the attention of the central and local governments and scientists (Trinh and Zablotskii, 2017; Tuyen et al., 2016). This study tested the efficiency of HSA in detecting UCFs from the Landsat-8 TIRS data in the Khanh Hoa coal field.

2.2 Data used

The images used in this study were the Landsat-8 (path 127, row 045) OLI (30-m spatial resolution) and TIRS (100-m spatial resolution) data acquired on 2nd December 2013, which were level L1TP product with precision and terrain correction. They were downloaded from the U.S. Geological Survey (USGS) website and projected in the UTM Zone N48 and WGS 1984 ellipsoid datum. In addition, eight UCF sites evenly distributed were collected from the field survey by retrospective study conducted on a group of people who had been

living next to the coal mining area in 2013. These coal fire sites were used for the validation of the fire areas delineated from the December 2013 Landsat-8 TIRS image. In addition, the ASTER Level 1 Precision Terrain Corrected Registered At-Sensor Radiance (ASTER) data acquired in October 2013 was also used to cross-validate those extracted from the Landsat-8 TIRS data.

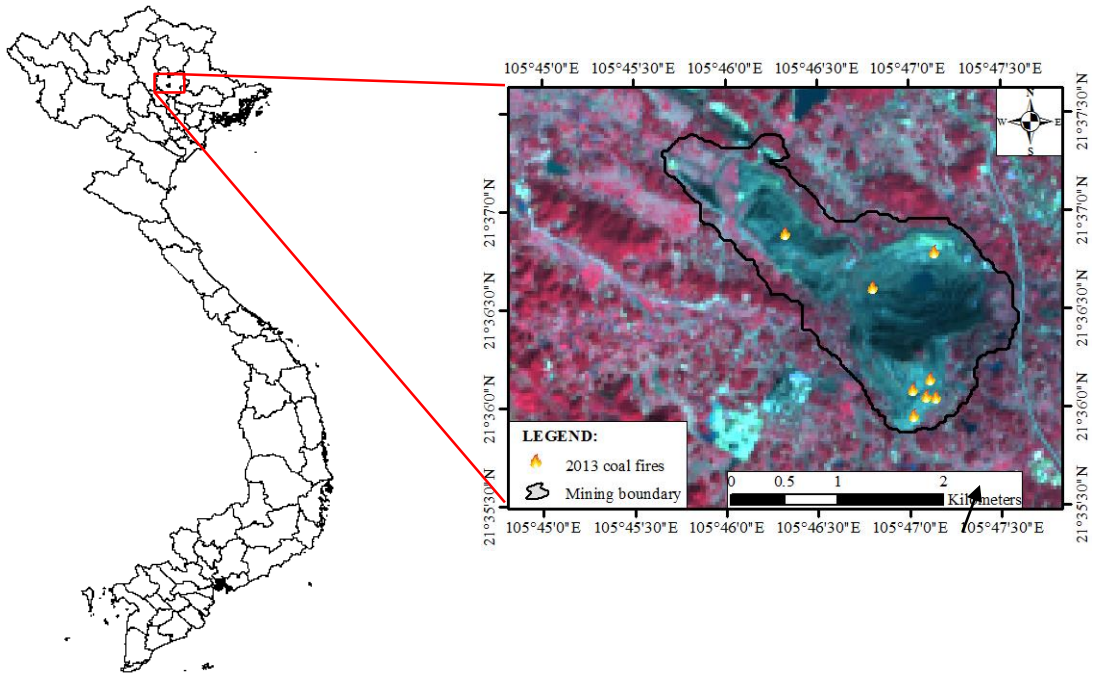

Figure 1. Study area of Khanh Hoa coal field, north-east of Vietnam (left) with false color composite (5,4,3) of Landsat 8 images acquired on 2nd December 2013 overlaid by mining boundary and known UCF sites (right).

2.3 Underground coal fire detection using HSA

The use of HSA to detect UCFs from the Landsat-8 TIRS data involved three main steps. Firstly, LSTs were retrieved from Landsat-8 thermal infrared data using the RTE. Secondly, HSA was carried out to measure the degree of spatial clustering among these LSTs. UCF areas were then delineated and computed based on 99 percent confidence level of hot spot areas. Finally, these fires were validated using known UCF sites collected from the field survey and were cross-validated by comparing with those obtained from the ASTER TIR data.

2.3.1 Land surface temperature retrieval from the Landsat-8 TIRS data

LST retrieval from the Landsat-8 TIRS data involves three main steps. The first step was the conversion from calibrated digital numbers (Q_{cal}) back to at-sensor spectral radiance using the following equation (Zanter, 2016):

$$L_{at-sensor,\lambda} = M_L Q_{cal} + \Delta_L \quad (1)$$

where $L_{at-sensor,\lambda}$ is the at-sensor radiance or Top of Atmospheric (TOA) radiance [W/(m^2/sr/µm)] at the wavelength λ (µm); M_L is the radiance multiplicative scaling factor for the band (RADIANCE_MULT_BAND_n from the metadata); Q_{cal} is the the quantized calibrated pixel value; Δ_L is the radiance additive scaling factor for the band (RADIANCE_ADD_BAND_n from the metadata);

The second step was the conversion of at-sensor spectral radiance to surface-leaving radiance by removing the effects of the atmosphere in the thermal region using the RTE-based approach (Barsi et al., 2003).

$$L_{at-sensor,\lambda} = \tau_\lambda[\varepsilon_\lambda B_{b,\lambda}(T_s) + (1-\varepsilon_\lambda)L^{\downarrow}_{atm,\lambda}] + L^{\uparrow}_{atm,\lambda} \quad (2)$$

where $L_{at-sensor,\lambda}$ is the at-sensor radiance [W/(m^2/sr/µm)] achieved in the first step; ε_λ is the land surface emissivity (LSE) and was derived based on the work of Sobrino et al. (2008); $B_{b,\lambda}(T_s)$ is the

blackbody radiance [W/(m^2/sr/µm)] given by the Planck's law and T_s is the LST (Kelvin); $L^{\uparrow}_{atm,\lambda}$ is the upwelling atmospheric radiance [W/(m^2/sr/µm)]; $L^{\downarrow}_{atm,\lambda}$ is the downwelling atmospheric radiance [W/(m^2/sr/µm)] and τ_λ is the total atmospheric transmissivity (dimensionless) between the surface and the sensor. The values of $L^{\uparrow}_{atm,\lambda}$, $L^{\downarrow}_{atm,\lambda}$ and τ_λ of 1.13, 1.89 and 0.85 were calculated using the web-based atmospheric correction tool developed by NASA for single thermal band sensors (Barsi et al., 2003).

Finally, the surface-leaving radiance was converted to LST by inversion of the Planck's law using equation (3):

$$T_s = \frac{K_2}{\ln\left[\frac{K_1}{B_{b,\lambda}(T_s)}+1\right]} \quad (3)$$

where K_2=calibration constant 2 (Kevin), K_1=calibration constant 1 [W/(m^2/sr/µm)], $B_{b,\lambda}(T_s)$=blackbody radiance [W/(m^2/sr/µm)], In=natural logarithm.

2.3.2 Hot spot analysis using Getis-Ord's G_i^* statistic

HSA characterizes the presence of hot spots (high clustered values) and cold spots (low clustered values) over an entire area by looking at each feature (LST value) within the context of its neighboring features. Therefore, after the LST was retrieved, the Getis-Ord's G_i^* statistic-based HSA was applied to identify the areas of high LST clusters which may be caused by the existence of UCFs. Ord and Getis (1995) defined a z-transformed form of Getis-Ord's G_i^* as follows:

$$G_i^*(d) = \frac{\sum_{j=1}^{n} w_{ij}(d)x_j - \bar{X}\sum_{j=1}^{n} w_{ij}(d)}{S\sqrt{\frac{n\sum_{j=1}^{n} w_{ij}^2(d) - (w_{ij}(d))^2}{n-1}}} \quad (4)$$

$$\text{with } \bar{X} = \frac{1}{n}\sum_{j=1}^{n} x_j \text{ and } S = \sqrt{\frac{\sum_{j=1}^{n} x_j^2}{n} - (\bar{X})^2}$$

where $G_i^*(d)$ is computed for feature (i) (the LST at location i in this study) at a distance (d) standardized as a z-score, x_j is the attribute value of each neighbor and $w_{ij}(d)$ represents the spatial weight for the target-neighbor i and j pair and n is the total number of samples in the dataset (Peeters et al., 2015).

High positive values of $G_i^*(d)$ and small p-values indicate a spatial clustering among high LSTs. Low negative values of $G_i^*(d)$ and small p-values denote spatial clustering for low LSTs. $G_i^*(d)$ values or z-scores near zero indicate no apparent spatial clustering. These Getis-Ord's G_i^* values and p-values define whether the location of a LST belongs to a hot spot (spatial cluster of high LSTs), a cold spot (spatial cluster of low LSTs) or an outlier (a high LST surrounded by low LSTs or vice versa). The Getis-Ord's G_i^* statistic computed by ArcGIS software is combined with the z-score into one single index called Getis z-scores (Mitchel, 2005). Very high or very low (negative) Getis z-scores, associated with very small p-values and are found in the tails of the normal distribution (Figure 2). For example, the Getis z-score represents the statistical significance of spatial clustering at a distance (d) (90% significant: >1.65 or <-1.65; 95% significant: >1.96 or <-1.96; 99% significant: >2.58 or <-2.58).

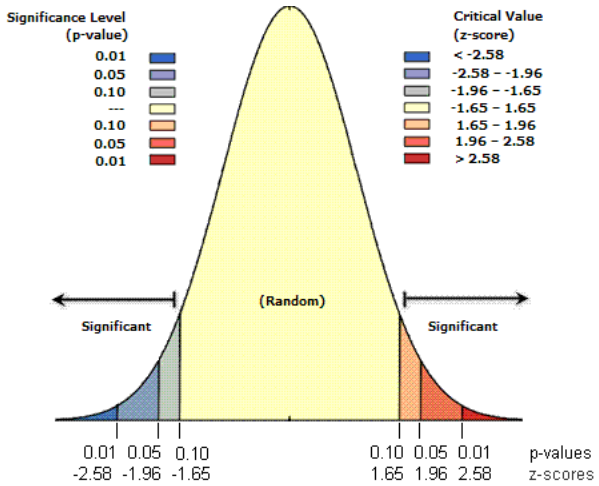

Figure 2. Visual interpretation of distribution of significance level (p-values) and z-score in ArcGIS (Mitchel, 2005).

2.3.3 Underground coal fire delineation

UCFs show a spatial clustering of high LSTs. These clusters are normally defined as points whose modulus of the Getis z-score is greater than a threshold value. In this study, if the Getis z-score of a pixel is greater than a threshold value of 2.58 corresponding to 99 percent confidence level, it is assigned a pixel of UCF. Based on a set of these Getis z-scores, four different levels of UCFs were categorized using statistical parameters (minimum, first quartile, median, third quartile and maximum

values). The validation of UCFs was finally carried out by overlapping known UCF sites on the coal fire areas delineated from the Landsat-8 TIRS data to assess the degree of consistency between them. In addition, the cross-validation of these fires was performed by comparing with those obtained from the October 2013 ASTER TIR data.

2.3.4. Data treatment with computer software

The statistical parameters (the minimum, first quartile, mean, median, third quartile and maximum values) and all plots (histogram, density trace, one-dimensional scatter, box-plot and empirical cumulative distribution function - ECDF) were created using StatDA, geoR and sgeostat packages of Statistical Modeling and Computing - R Language (version i386 3.5.1) (Team, 2016). The LST was retrieved from the Landsat-8 TIRS and ASTER TIR data using ENVI image analysis software (version 5.2). All of the maps and the Getis z-score were produced and computed using GIS software (ArcGIS version 10.3).

3. RESULTS AND DISCUSSION

3.1 Land surface temperatures in the Khanh Hoa coal field

The distribution of LSTs retrieved from the December 2013 Landsat-8 TIRS data in the study area is shown in Figure 3 and 4. The minimum, median, mean and maximum values of these LSTs are 19.0, 24.7, 24.9 and 36.5ºC respectively. Figure 3(a) shows a strongly right-skewed distribution of the LST dominated by many very high values (high LSTs). The distribution of the LST was obviously not normal but extremely skewed to the right. As a result, the typical S-shape for the ECDF plot (Figure 3(b)) was not present. The ECDF plot of the LST shows a big the distance of these high LSTs from the main body of the data. In general, high LSTs were found inside of the Khanh Hoa mining boundary whilst low LSTs were found outside of the coal field such as in mountainous areas and Nui-Coc Lake in the southwest region. These high LSTs were higher than those of surrounding environments of more than 10ºC which were thermal anomalies caused by UCFs. Most of LSTs at the hottest points of the ground surface were above the fire exceeded 30°C and were near areas of active UCF sites (Figure 4).

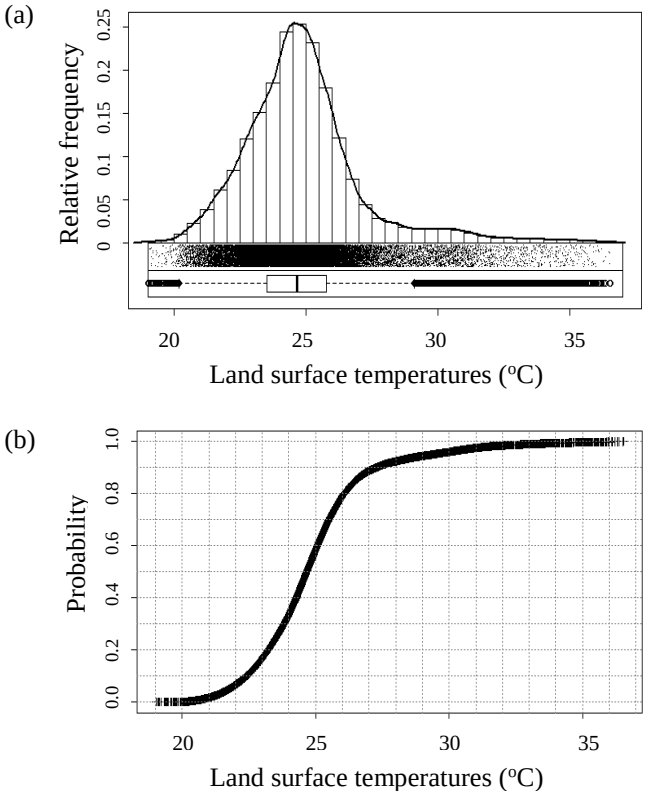

Figure 3. Histogram, density trace, one-dimensional scatterplot, boxplot (a) and empirical cumulative density function plot (b) of LSTs.

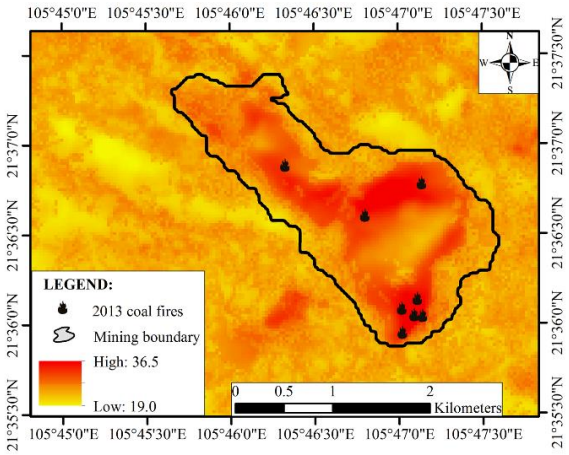

Figure 4. LSTs retrieved from the Landsat-8 TIRS data in the Khanh Hoa coal field.

3.2 Hot spot analysis

The Getis-z score distributions are shown in Figure 5 and 6. The minimum, median, mean and maximum values of Getis z-scores are -5.74.0, -0.22, 0 and 11.4 respectively. Similar to those obtained from the LST, the distribution of the Getis z-score was also strongly right-skewed due to the existence

of very high values detected near UCF sites (Figure 6(a)). The typical S-shape for the ECDF plot of the Getis z-score (Figure 6(b)) was not present. A big distance between high values of Getis z-scores from the main body of the data was found in the ECDF plot. These high Getis z-scores were detected in the areas where their LSTs were high.

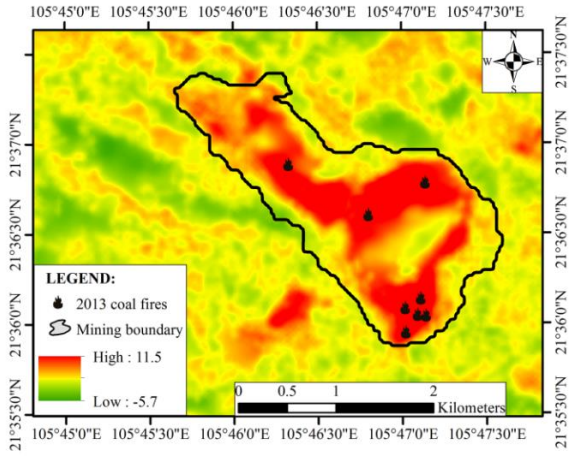

Figure 5. Spatial distribution of Getis z-scores in the Khanh Hoa coal field.

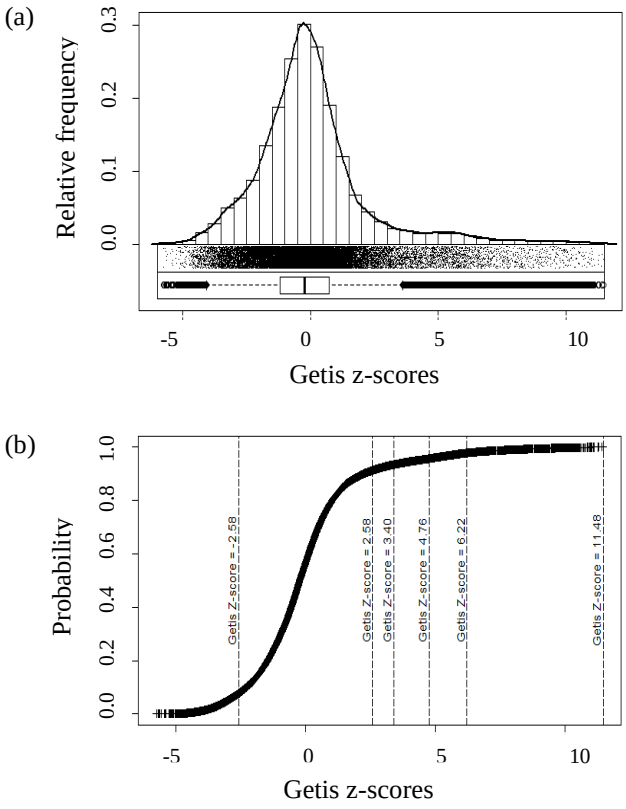

Figure 6. Histogram, density trace, one-dimensional scatterplot, boxplot (a) and empirical cumulative density function plot (b) of Getis z-scores.

The distribution of hot spots (spatial clustering among high LSTs) and cold spots (spatial clustering for low LSTs) in the Khanh Hoa coal field is shown in Figure 7 and their areas are summarized in Table 1. The total area of hot spots was 358 hectares, accounting for 17% of the total area. Survey results indicated that these hot spots were mainly concentrated in the mining area where their LSTs were higher than those of the surrounding environment. An area of hot spots was also found outside the mining area which was mostly concentrated in the residential area or industrial factories. A total hot spot area of 236.9 hectares with a 99 percent confidence level was detected and completely located in the coal field, accounting for 67% of the total area. In particular, these hot spots coincided perfectly with known UCFs sites in the study. The total area of cold spots was 463.4 hectares, accounting for 17% of the total area. These cold spots were mainly detected outside the coal mine and were concentrated in mountainous areas with a highly dense vegetation and water surface. The remaining 70% were non-significant spatial clusters. It can be seen that high Getis z-scores were higher than those of surrounding environments, especially for 99% confident level hot spot areas. It is therefore these hot spots were selected to identify UCFs in the Khanh Hoa coal field.

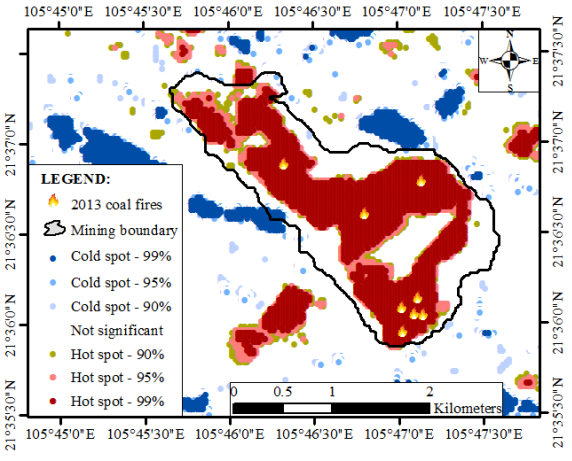

Figure 7. Hot spots and cold spots obtained from the 2nd December 2013 Landsat-8 TIRS data.

3.3 Underground coal fire delineation

The minimum, first quartile, median, mean, third quartile and maximum values of the 99% confident level of Getis z-scores are 2.58, 3.40, 4.76, 6.22 and 11.48 respectively.

Table 1. Summary table of hot spot and cold spot areas.

No	Confidence level	Cold spot areas (hectares)	Hot spot areas (hectares)
1	90%	109.0	48.4
2	95%	147.5	72.7
3	99%	206.9	236.9
4	Sum	463.4	358.0

Four different levels of UCFs were categorized as low, medium, high and extremely high levels. The distribution of these fires is shown in Figure 8. The total area of UCFs was 197 hectares, accounting for 46.9% of the coal field area, of which the areas of low, medium, high and extremely high coal fire levels were 37.3, 47.3, 53.2 and 59.3 hectares respectively.

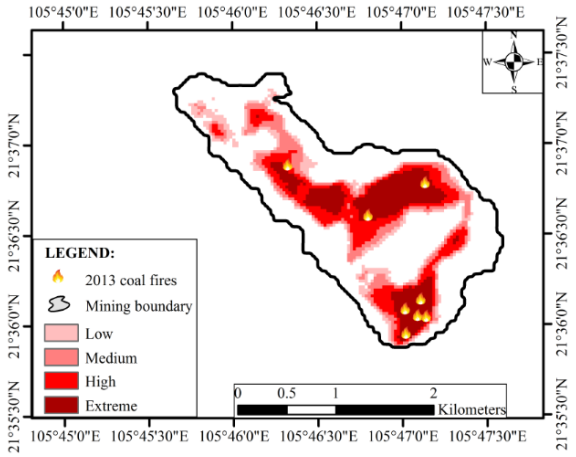

Figure 8. The UCF degree extracted from the 2nd December 2013 Landsat-8 TIRS data.

The extremely high-level of UCFs, accounting for 14.1%, was mainly concentrated in the central and southern areas, especially in the area of the coal ash dump. The locations of extremely high level UCFs coincided with all known UCF sites collected from the field survey. The high level of coal fires occupied the second largest area, accounting for 12.7% of the coal field area. These fires were also found mainly in the center and in the coal ash dump area of the southern mining area, and adjacent to the extremely high level of fires. The medium level of fires accounted for 11.3% of the coal field area. These fires were observed not only near the center and south of the coal field and had spread to the northwest of the coal field with a relatively large area. Low-level coal fires constituted only 18.9% of the mining area and were largely observed in the northwest of the coal field. It can be seen that UCFs were mainly detected in the central area and in the area of the coal ash dump, south of the coal field.

The UCFs detected from the Landsat-8 TIRS data were in the northern, southern and north-western areas of the Khanh Hoa coal field and covered entirely with eight coal fire sites. In addition, LSTs of these UCF areas retrieved from the 7th October 2013 ASTER TIR data were higher than those of surrounding environments of more than 10°C (Figure 9). Cross-validation of these fires with those extracted from the October ASTER TIR image also showed a high consistency (Figure 10). Although a smaller area of UCFs was detected from the ASTER TIR image when compared with those obtained from the Landsat-8 TIRS image, these UCFs mostly covered over all known UCF sites. This difference was due to the high ambient temperatures (as shown Figure 9) resulting in difficulty in the UCF detection using the autumn-acquired image.

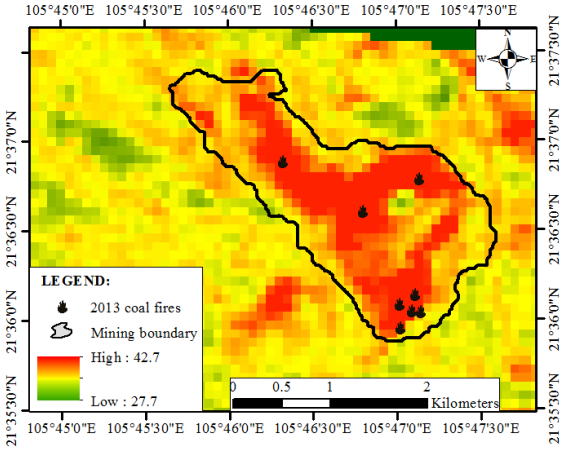

Figure 9. LSTs retrieved from the 7th October 2013 ASTER TIR data.

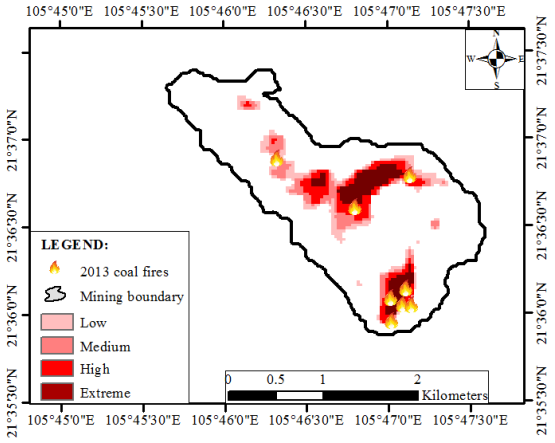

Figure 10. The UCF degree extracted from the 7th October 2013 ASTER TIR data.

4. CONCLUSIONS

This study presents a method for UCF detection from the Landsat-8 TIRS data using HSA which accounts for the degree of spatial autocorrelation among LSTs. LSTs were firstly extracted from the Landsat-8 TIRS data using the RTE. Based on these LSTs, the degree of spatial clustering among them was measured by means of HSA. UCF areas were then delineated from 99 percent confidence level of hot spot areas and were finally validated using eight known UCF sites. The results from the Khanh Hoa coal field showed that UCFs extracted from the 2nd December 2018 Landsat-8 TIRS data coincided perfectly with all known UCFs. These UCFs were highly consistent with those extracted from the 7th October 2018 ASTER TIR data. A total fire area of 197 hectares were detected, of which the areas of low, medium, high and extremely high coal fire levels were 37.3, 47.3, 53.2 and 59.3 hectares respectively. These fires were mainly concentrated in the central area, in coal ash dump sites and north-west of the coal field. These findings indicate HSA is an effective method for detecting UCFs from the Landsat-8 TIRS data. However, data presented in this study were acquired in winter and autumn. Further research work is needed on the use of remotely sensed images acquired in different seasons such as summer and spring. Moreover, more experiments on typical coal fields presented in previous studies such as India's Jharia coal field (Pal et al., 2016; Roy et al., 2015a; Roy et al., 2015b; Singh et al., 2017) and China's Wuda (Song et al., 2015) and Rujigou coal fields (Huo et al., 2014a; Huo et al., 2014b) are necessary to test the effectiveness of HSA in UCF detection.

ACKNOWLEDGEMENTS

This work is sponsored and financed by the Ministry-level Scientific and Technological Key Programs of Ministry of Natural Resources and Environment of Vietnam under the project "Application of thermal infrared remote sensing and GIS for mapping underground coal fires in Quang Ninh coal basin" (Grant number TNMT.2017.08.06). Authors would like to thank the editors and two anonymous reviewers for their constructive comments which helped us to improve the manuscript and the people who lived near the Khanh Hoa coal mining sites for their help during the field survey.

REFERENCES

Abbas MR, Ahmad BB, Abbas TR. Use MODIS satellite data to study new phenomena of underground fire in the Al Ruhban oasis in Al Najaf city, Iraq. Environmental Earth Sciences 2015;73:3475-85.

Barsi JA, Barker JL, Schott JR. An atmospheric correction parameter calculator for a single thermal band earth-sensing instrument. Proceedings of the International Geoscience and Remote Sensing Symposium (IGARSS); 2003 Jul 21-25; Toulouse, France: New York: IEEE; 2003.

Bhattacharya A, Reddy S, Mukherjee T. Multi-tier remote sensing data analysis for coal fire mapping in Jharia coal field of Bihar, India. Proceedings of the Twelfth Asian Conference on Remote Sensing; 1991 30th Oct - 5th Nov; National University of Singapore, Singapore: 1991.

Chatterjee A, Bhattacharya A, Mukherjee A, Pramanik T. Study of coal mine fire in Damodar River basin, India using thermal remote sensing technique. Proceedings of the 38th COSPAR Scientific Assembly; 2010 July 15-18; Bremen, Germany: 2010.

Chatterjee R. Coal fire mapping from satellite thermal IR data-a case example in Jharia Coal field, Jharkhand, India. ISPRS Journal of Photogrammetry and Remote Sensing 2006;60:113-28.

Ding L, Chen K-L, Liu T, Cheng S-G, Wang X. Spatial-temporal hotspot pattern analysis of provincial environmental pollution incidents and related regional sustainable management in china in the period 1995-2012. Sustainability 2015;7:14385-407.

Dozier J. A method for satellite identification of surface temperature fields of subpixel resolution. Remote Sensing of Environment 1981;11:221-9.

Du X, Bernardes S, Cao D, Jordan TR, Yan Z, Yang G, Li Z. Self-adaptive gradient-based thresholding method for coal fire detection based on ASTER data - Part 2, validation and sensitivity analysis. Remote Sensing 2015a;7:2602-26.

Du X, Cao D, Mishra D, Bernardes S, Jordan TR, Madden M. Self-adaptive gradient-based thresholding method for coal fire detection using ASTER thermal infrared data, part I: methodology and decadal change detection. Remote Sensing 2015b;7:6576-610.

Finkelman R, Stracher G. Environmental and health impacts of coal fires. In: Stracher GB, Prakash A, Sokol EV, editors. Coal and Peat Fires: A Global Perspective: Volume 1: Coal-Geology and Combustion. English: Elsevier Science; 2011. p. 115-25.

Gangopadhyay PK, Lahiri-Dutt K, Saha K. Application of remote sensing to identify coalfires in the Raniganj Coalbelt, India. International Journal of Applied Earth Observation and Geoinformation 2006;8:188-95.

Greene GW, Moxham RM, Harvey AH. Aerial infrared surveys and borehole temperature measurements of

coal mine fires in Pennsylvania. Proceedings of the Sixth International Symposium on Remote Sensing of Environment, Volume II. Held; 1969 Oct 13-16; University of Michigan, USA: 1969

Huijun D, Shijun H, Jie F. The detection method of fire abnormal based on directional drilling in complex conditions of mine. Proceedings of the 4th International Conference on Energy Materials and Environment Engineering (ICEMEE 2018); 2018 Sep 28-30; Zhuhai, China: 2018.

Huo H, Jiang X, Song X, Li Z-L, Ni Z, Gao C. Detection of coal fire dynamics and propagation direction from multi-temporal nighttime Landsat SWIR and TIR data: A case study on the Rujigou coalfield, Northwest (NW) China. Remote Sensing 2014a;6:1234-59.

Huo H, Jiang X, Song X, Ni Z, Liu L. Coal fires dynamics detection over Rujigou coalfield, Ningxia, NW China. Proceedings of the IEEE Geoscience and Remote Sensing Symposium (IGARSS); 2014 July 13-18; Quebec City, Canada: 2014b.

Huo H, Ni Z, Gao C, Zhao E, Zhang Y, Lian Y, Zhang H, Zhang S, Jiang X, Song X, Zhou P, Cui T. A study of coal fire propagation with remotely sensed thermal infrared data. Remote Sensing 2015;7:3088-113.

Jiang W-g, Gu L, Yang B, Chen Q. Monitoring method of underground coal fire based on night thermal infrared remote sensing technology. Spectroscopy and Spectral Analysis 2011;31:357-61.

Cheng KL, Hsu SC, Li WM, Ma HW. Quantifying potential anthropogenic resources of buildings through hot spot analysis. Resources, Conservation and Recycling 2018;13:10-20.

Kuenzer C, Dech S. Thermal Infrared Remote Sensing: Sensor, Methods, Applications. New York: Springer; 2014.

Kuenzer C, Zhang J, Li J, Voigt S, Mehl H, Wagner W. Detecting unknown coal fires: synergy of automated coal fire risk area delineation and improved thermal anomaly extraction. International Journal of Remote Sensing 2007;28:4561-85.

Kuenzer C, Zhang J, Sun Y, Jia Y, Dech S. Coal fires revisited: The Wuda coal field in the aftermath of extensive coal fire research and accelerating extinguishing activities. International Journal of Coal Geology 2012;102:75-86.

Künzer C, Zhang J, Tetzlaff A, Voigt S, Wagner W. Automated demarcation, detection and quantification of coal fires in China using remote sensing data. In: Stefan V, Horst R, Li JH, Li J, Jayakumar R, editors. Spontaneous Coal Seam Fires: Mitigating a Global Disaster. Beijing: Tsinghua University Press; 2008. p. 362-80.

Lu D, Song K, Zang S, Jia M, Du J, Ren C. The effect of urban expansion on urban surface temperature in Shenyang, China: an analysis with landsat imagery. Environmental Modeling and Assessment 2015; 20:197-210.

Mitchel A. The ESRI Guide to GIS analysis, Volume 2: Spartial Measurements and Statistics. 1st ed. California, USA: ESRI Press; 2005.

Nguyen TT. Use of Moran's I and robust statistics to separate geochemical anomalies in Jiurui area (Southeast China). Maden Tetkik ve Arama Dergisi 2018;156:181-94.

Nguyen TT, Vu DT, Trinh LH, Nguyen TLH. Spatial cluster and outlier identification of geochemical association of elements: A case study in Juirui copper mining area. Bulletin of the Mineral Research and Exploration 2016;153:159-67.

Obida CB, Blackburn GA, Whyatt JD, Semple KT. Quantifying the exposure of humans and the environment to oil pollution in the Niger Delta using advanced geostatistical techniques. Environment International 2018;111:32-42.

Odland J. Spatial autocorrelation. California, USA: Sage Publications; 1988.

Ord JK, Getis A. Local spatial autocorrelation statistics: distributional issues and an application. Geographical Analysis 1995;27:286-306.

Pal S, Vaish J, Kumar S, Bharti AK. Coal fire mapping of East Basuria Colliery, Jharia coalfield using vertical derivative technique of magnetic data. Journal of Earth System Science 2016;125:165-78.

Pandey J, Kumar D, Panigrahi D, Singh V. Temporal transition analysis of coal mine fire of Jharia coalfield, India, using Landsat satellite imageries. Environmental Earth Sciences 2017;76:439.

Peeters A, Zude M, Käthner J, Ünlü M, Kanber R, Hetzroni A. Getis-Ord's hot-and cold-spot statistics as a basis for multivariate spatial clustering of orchard tree data. Computers and Electronics in Agriculture 2015;111:140-50.

Qi G, Wang D, Zheng K, Xu J, Qi X, Zhong X. Kinetics characteristics of coal low-temperature oxidation in oxygen-depleted air. Journal of Loss Prevention in the Process Industries 2015;35:224-31.

Roy P, Guha A, Kumar KV. An approach of surface coal fire detection from ASTER and Landsat-8 thermal data: Jharia coal field, India. International Journal of Applied Earth Observation and Geoinformation 2015a;39:120-7.

Roy P, Guha A, Kumar KV. Structural control on occurrence and dynamics of Coalmine fires in Jharia Coalfield: a remote sensing based analysis. Journal of the Indian Society of Remote Sensing 2015b;43:779-86.

Saini V, Gupta RP, Arora MK. Environmental impact studies in coalfields in India: A case study from Jharia coal-field. Renewable and Sustainable Energy Reviews 2016;53:1222-39.

Singh A, Raju A, Pati P, Kumar N. Mapping of coal fire in Jharia coalfield, India: A Remote Sensing Based Approach. Journal of the Indian Society of Remote Sensing 2017;45:369-76.

Sobrino JA, Jiménez-Muñoz JC, Sòria G, Romaguera M, Guanter L, Moreno J. Land surface emissivity retrieval from different VNIR and TIR sensors. IEEE Transactions on Geoscience and Remote Sensing 2008;46:316-27.

Song Z, Kuenzer C. Spectral reflectance (400-2,500 nm) properties of coals, adjacent sediments, metamorphic and pyrometamorphic rocks in coal-fire areas: A case study of Wuda coalfield and its surrounding areas, Northern China. International Journal of Coal Geology 2017;171:142-52.

Song Z, Kuenzer C, Zhu H, Zhang Z, Jia Y, Sun Y. Analysis of coal fire dynamics in the Wuda syncline impacted by fire-fighting activities based on in-situ observations and Landsat-8 remote sensing data. International Journal of Coal Geology 2015;141:91-102.

Stopka TJ, Goulart MA, Meyers DJ, Hutcheson M, Barton K, Onofrey S. Identifying and characterizing hepatitis C virus hotspots in Massachusetts: A spatial epidemiological approach. BMC Infectious Diseases 2017;17:294.

Su H, Zhou F, Qi H, Li J. Design for thermoelectric power generation using subsurface coal fires. Energy 2017;140:929-40.

Team RC. R: A language and environment for statistical computing. R Foundation for Statistical Computing, Vienna, Austria [Internet]. 2016. Available from: ftp://ftp.uvigo.es/CRAN/web/packages/dplR/vignettes/intro-dplR.pdf.

Tobler WR. Smooth pycnophylactic interpolation for geographical regions. Journal of the American Statistical Association 1979;74:519-30.

Tran DX, Pla F, Latorre-Carmona P, Myint SW, Caetano M, Kieu HV. Characterizing the relationship between land use land cover change and land surface temperature. ISPRS Journal of Photogrammetry and Remote Sensing 2017;124:119-32.

Tran VT, Tran DK, Phan QV. Exploitation and management of burning coal seams in underground mines of Vietnam. Proceedings of the Second International Conference on Coal Fire Research (ICCFR 2); 2010 May 19-21; Berlin, Germany: 2010.

Trinh LH, Zablotskii V. The application of LANDSAT multi-temporal thermal infrared data to identify coal fire in the Khanh Hoa coal mine, Thai Nguyen province, Vietnam. Izvestiya, Atmospheric and Oceanic Physics 2017;53:1081-7.

Tuyen LT, Tuan NV, Ohga K, Isei T. Characteristics of spontaneous combustion of Anthracite in Vietnamese coal mines. Journal of the Mining and Materials Processing Institute of Japan 2016;132:167-74.

Voigt S, Tetzlaff A, Zhang J, Künzer C, Zhukov B, Strunz G. Integrating satellite remote sensing techniques for detection and analysis of uncontrolled coal seam fires in North China. International Journal of Coal Geology 2004;59:121-36.

Vu HN. Assessment of the Environmental Status in Khanh Hoa Coal Field, Thai Nguyen Province [dissertation]. Thai Nguyen, Vietnam: Thai Nguyen University of Agriculture and Forestry; 2013.

Yang B, Chen Y, Li J, Gong A, Kuenzer C, Zhang J. Simple normalization of multi-temporal thermal IR data and applied research, on the monitoring of typical coal fires in northern China. Proceedings of the Geoscience and Remote Sensing Symposium; 2005 July 29-29; Seoul, South Korea: 2005.

Zanter K. Landsat 8 (L8) data users handbook. Landsat Science Official Website. 2016. Available from: https://landsat. usgs. gov/landsat-8-l8-data-users-handbook.

Zhang H, Tripathi NK. Geospatial hot spot analysis of lung cancer patients correlated to fine particulate matter (PM2.5) and industrial wind in Eastern Thailand. Journal of Cleaner Production 2018; 170:407-24.

Zhang X, Cassells C, Van Genderen J. Multi-sensor data fusion for the detection of underground coal fires. Geology and Mining 1998;77:117-28.